ISME

The Effect of Repeated Impact Loading on Reservoir Rock Properties

M. Naderan Tahan[*]
PhD Student

Kh. Naderan Tahan[†]
Professor

S.S. Bahrainian[‡]
Associate Professor

The objective of this paper is to present the results of a research program launched to investigate the mechanism and amount of changes of reservoir rock properties due to pulse stress waves. These waves are induced in cylindrical samples by applying repeated impact loading along the sample axes in a falling weight testing apparatus. After each step of loading, permeability, effective porosity, wave velocities are measured by standard methods and CT images are prepared. Results show that if the amplitude of dynamic stress exceeds the dynamic fracture strength and spall strength of the samples, micro fracture will emerge and permeability will increase significantly while the effective porosity decreases at first steps of loading but, recovers during the subsequent steps. Emerging and growth of new fractures are visible in CT images, too. Total energy consumption prior to complete breakage, and the strain rate of incident wave, affect the results.

DOI: 10.30506/jmee.2020.115766.1204

Keywords: dynamic fracture strength, effective porosity, impact loading, permeability, reservoir rock, spallation.

1 Introduction

Reservoir rock is a natural porous medium with interconnected and isolated pores and fractures that contain hydrocarbons as fluid and gas under ambient pressure. The content of the reservoir is extracted through oil wells, partially. In order to extract the remaining part of hydrocarbon which is trapped in isolated pores and fractures, induced fracturing is a traditional way of creating new fracture networks, connecting isolated pores and districts, and opening and extending existing fractures. A conceptual illustration of a reservoir rock structure before and after induced fractures due to impact loading is indicated in Figure (1). The interest in reservoir fracturing dates back to 1859, since the first oil well digging in Pennsylvania. Increased oil production was observed by explosions at the bottom of oil wells [1]. Reservoir fracturing provides a better connection of the natural fracture system with well bore, leading to improve some of the reservoir rock properties [2, 3].

[*]PhD Student of Mechanical Engineering Department, Faculty of Engineering, Shahid Chamran University of Ahvaz, Ahvaz, Iran m-naderan@scu.ac.ir

[†]Corresponding Author, Professor of Mechanical Engineering Department, Faculty of Engineering, Shahid Chamran University of Ahvaz, Ahvaz, Iran naderan_k@scu.ac.ir

[‡]Associate Professor of Mechanical Engineering Department, Faculty of Engineering, Shahid Chamran University of Ahvaz, Ahvaz, Iran bahrainian@scu.ac.ir

Receive : 2019/10/28 Accepted : 2020/06/18

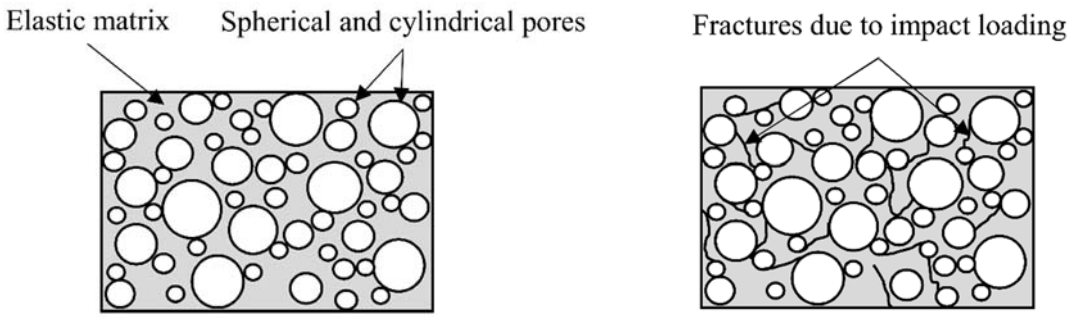

Figure 1 Conceptual illustration of reservoir rock sample: **(a)** idealized model with different size spherical and cylindrical pores before impact loading, **(b)** after impact loading

Various chemical methods and hydraulic and waterless fracturing techniques, employed to increase the productivity of reservoirs, are known as reservoir stimulation methods for Enhanced Oil Recovery (EOR) or Improved Oil Recovery (IOR) operation [4-6]. The application of mechanical methods for reservoir stimulation is considered in the tertiary stage of EOR. In one of these methods, suitable stress waves are induced in the reservoir that will affect some of its properties [7, 8]. Fracturing is primarily the result of exceeding compressive, shear, and tensile stress from its corresponding strength. Typical rock strengths for these stresses vary in the order of 100, 10 and 1, respectively [9]. If at a point within a material, the magnitude of a tensile stress field due to high strain rate exceeds the tensile strength (dynamic fracture strength criterion), cracks will appear [10]. The response of materials and structures to high strain rate loading is usually very complex, involving deformation of the medium and sometimes fracturing or disintegration [11-13]. On the other hand, the effect of stress waves induced by impact loading on a porous material leading to fracture of matrix, generating new surfaces or increasing pores (activating isolated pores), depends on the strain rate and the initial porosity of the material [14-16]. Although, the factors affecting strength of some porous rocks under repeated impact loading are discussed in recent works [17, 18] but little attention is paid in the literature on the variations of absolute gas permeability and effective porosity of reservoir rock under such loading. The subject of stress wave propagation in isotropic elastic media is well covered in [19-21], while a theory considering wave motion in porous media is developed in [22]. Compressive stress waves interact with free surfaces of pores and fractures through the superposition of its reflected part with that part of which is not reflected yet, producing a tensile stress wave. If certain conditions are fulfilled, "spalling" will occur due to this stress wave [23]. Spall is a tensile failure that results from the nucleation, growth, and coalescence of micro fractures or micro voids produced in concentration of the order of $10^6/cm^3$ when large stresses are imposed for short times. Because of the short duration of load application, the maximum tensile stress attained during the spall process is usually greatly in excess of the stress that produce fracture under static loading. On the other hand, the tensile stress at which micro fracture or micro void nucleation begins is generally equal to the static value [24].

Although in treating the spall fracture theory, usually the outside surface of material is considered as capable surface for reflecting the compressive stress waves [23, 25] but we believe that the surfaces of cracks and pores within the reservoir rock also can be considered as potential surfaces for this phenomenon. Idealizing these surfaces by flat, spherical and cylindrical surfaces will help the understanding of the event theoretically. Detailed governing equations of stress field near the free surfaces of flat, spherical, and cylindrical cavities regarding compressive harmonic waves are derived and discussed in [20, 21, 26, and 27].

The objective of this paper is to present the results of a research program launched to investigate the mechanism and amount of changes of reservoir rock parameters due to pulse stress waves. In this research, pulse stress waves are induced in cylindrical samples of reservoir rock by applying repeated impact loading along the sample axes in a falling weight testing apparatus. The compressive stress waves produced by impact loading, incident on and reflect from stress free surfaces of pores and fractures, under certain conditions may cause spallation. The pore walls will break due to spallation and stress concentration, creating new micro fracture networks, that leads to changes in rock properties.

Three reservoir rock core plugs from Ahvaz Asmari formation in south-west of Iran are considered as test samples. The samples are dry and free from any fluid and no confining pressure. After each step of successive loading, absolute gas permeability, effective porosity, longitudinal and shear wave velocities within the samples are measured by standard methods and equipment and CT images are prepared. In studying the theoretical aspects, a meso-mechanics approach is considered where the behavior of the individual voids or cracks are averaged over a relevant volume element (RVE) which represents a continuum point in space (in this paper a core plug) [23]. A brief review of the elastic stress wave interaction with free flat and spherical surfaces is presented in order to show the existence of a point near the stress free surfaces where the maximum tensile stress appear, hence a potential location for spallation.

2 Interaction of one dimensional elastic stress waves with free surfaces

Consider a compressive harmonic stress wave, described by $\sigma(x,t)=-a\sin(kx-\omega t)$, incidents onto a flat free surface of a semi-infinite elastic solid. After reflection, it converts to a tensile stress wave $\sigma(x,t)=a\sin(-kx-\omega t)$. Combination of these two stress waves at any point of medium is represented by:

$$\sigma(x,t)=-a\sin(kx-\omega t)+a\sin(-kx-\omega t)=-2a\sin kx\cos\omega t \tag{1}$$

In this equation a, k, ω, x and t are amplitude, wave number, frequency, distance travelled by the wave and time, respectively. The amplitude of scattered field becomes maximum for $kx=(2m+1)\pi/2$ (m is an integer). Since $k=2\pi/\lambda$, minimum distance from free surface where maximum stress would appear, is equal to $x=\lambda/4$. Figure (2) (a-c) show the incidence and reflection of a harmonic compressive stress wave in three steps for t=0. Scattering of this wave after a time delay is illustrated in Figure (2) (d). Although the wave shape will affect to some extent the result of analysis, but since any wave shape can be resolved into series of harmonic waves with different frequencies and amplitudes, a similar analysis may be applied to other wave shapes. Radial and shear components of a scattered stress field around a spherical cavity with radius $r=a$, in an infinite elastic solid are derived as follows [21]:

$$\sigma_{rr}=(2\mu/r)\sum_{n=0}^{\infty}(-\varphi_0\varepsilon_3+A_n\varepsilon_{31}+B_n\varepsilon_{32})P_n$$
$$\sigma_{r\theta}=(2\mu/r)\sum_{n=0}^{\infty}(-\varphi_0\varepsilon_4+A_n\varepsilon_{41}+B_n\varepsilon_{42})\frac{dP_n}{d\theta} \tag{2}$$

Where μ is the shear modulus of elastic media, A_n and B_n are constant coefficients, φ_0 is the amplitude of incident potential function and $P_n=P_n(\cos\theta)$ is Legendre function. Other functions are defined as follow:

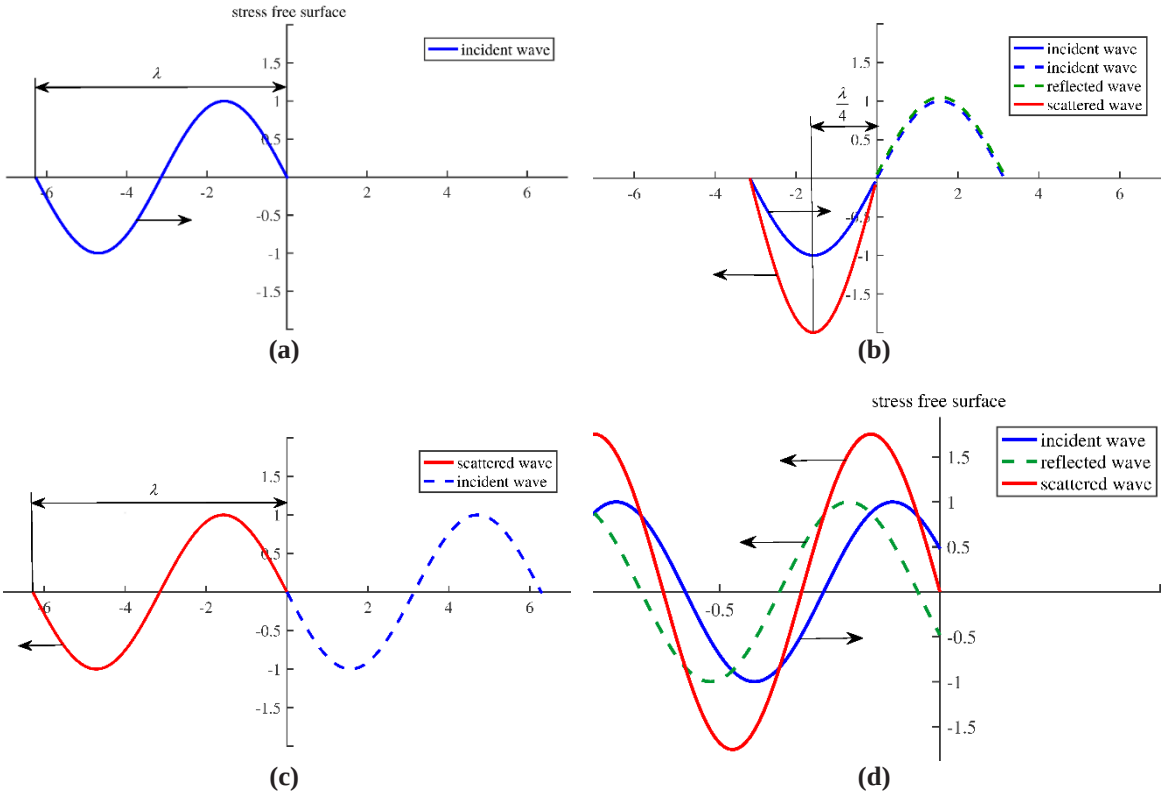

Figure 2 wave profiles when an incident harmonic wave of length λ is reflected from a flat free surface for zero time **(a, b, c)** and after a time delay **(d)**

$$
\begin{aligned}
\varepsilon_3 &= -i^n(2n+1)[(n^2-n-\frac{1}{2}\beta^2r^2)\,j_n(\alpha r)+2\alpha r j_{n+1}(\alpha r)]\\
\varepsilon_4 &= -i^n(2n+1)[(n-1)\,j_n(\alpha r)-\alpha r j_{n+1}(\alpha r)]\\
\varepsilon_{31} &= (n^2-n-\frac{1}{2}\beta^2r^2)h_n(\alpha r)+2\alpha r h_{n+1}(\alpha r)\\
\varepsilon_{41} &= (n-1)h_n(\alpha r)-\alpha r h_{n+1}(\alpha r)\\
\varepsilon_{32} &= -n(n+1)[(n-1)h_n(\beta r)-\beta r h_{n+1}(\beta r)]\\
\varepsilon_{42} &= -(n^2-1-\frac{1}{2}\beta^2r^2)h_n(\beta r)-\beta r h_{n+1}(\beta r)
\end{aligned}
\tag{3}
$$

In these equations j_n and h_n are first kind spherical Bessel and Hankel functions, $\alpha = k_l = \omega\sqrt{\rho/(\lambda+2\mu)}$ and $\beta = k_t = \omega\sqrt{\rho/\mu}$ are longitudinal and transverse wave number, ω is frequency, λ and μ are Lame' coefficients and ρ is density of medium. By considering $E_i = \varepsilon_i|_{r=a}, E_{ij} = \varepsilon_{ij}|_{r=a}$ constant coefficients A_n and B_n can be calculated from the following system of Eq.s (4) and (5):

$$
\begin{bmatrix} E_{31} & E_{32} \\ E_{41} & E_{42} \end{bmatrix}\begin{bmatrix} A_n \\ B_n \end{bmatrix} = \varphi_0 \begin{bmatrix} E_3 \\ E_4 \end{bmatrix} \tag{4}
$$

$$
A_n = \frac{\varphi_0(E_3E_{42}-E_4E_{32})}{(E_{31}E_{42}-E_{32}E_{41})}, \qquad B_n = \frac{\varphi_0(E_4E_{31}-E_3E_{41})}{(E_{31}E_{42}-E_{32}E_{41})} \tag{5}
$$

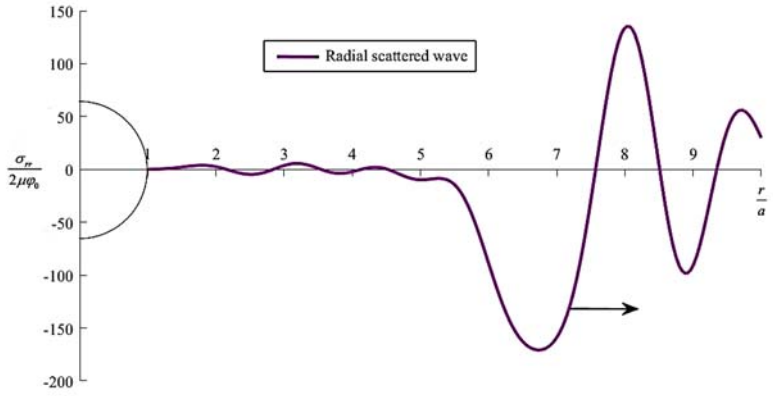

Figure 3 Normal stress wave along radial axes leaving a spherical cavity in an infinite elastic solid

Considering a plane passing through the center of the cavity, the non-dimensional radial stress at points located on radial axes and away from the cavity surface are calculated and drawn in Figure (3). Maximum of total stress field is located at $r/a \approx 6.75$ for specified iteration number (*n=30*).

3 Impact loading

3. 1 Drop weight loading

Impact loading is imposed on core plugs using a drop weight apparatus. Figure (4) shows a schematic diagram of the apparatus. It consists of a fixed base, two vertical columns and two transverse members. The upper member is fixed and the lower one slides along the columns carrying the steel falling weight or impactor. The sample sits between two steel caps during tests in order to avoid direct crash.

If the weight *W* falls from a height *h* on the sample with stiffness *k*, the equivalent static force *F* exerted on the sample is [28]:

$$F = W + W\sqrt{1 + 2hk/W} \tag{6}$$

The stiffness, *k*, is the ratio of measured ultimate static load, to the total deflection, which are obtained from uniaxial compression test. A compressive stress, σ_c corresponding to the equivalent static force *F* can be calculated for each impact loading. The weight *W* strikes the steel cap with thickness t, at velocity $V = \sqrt{2gh}$, and produces in it a strain rate $\dot{\varepsilon}_{steel}$. Due to the difference of acoustic impedances of steel cap and rock samples, only a part of this strain rate, $\dot{\varepsilon}_{rock}$, is transferred into the sample which is calculated by considering a transmission coefficient *T* as fallows [29]:

$$T = 2I_2/(I_1 + I_2),\ I = \rho c_L \approx \sqrt{\rho E} \tag{7}$$

$$\dot{\varepsilon}_{steel} = V/t, \dot{\varepsilon}_{rock} = T\dot{\varepsilon}_{steel} \tag{8}$$

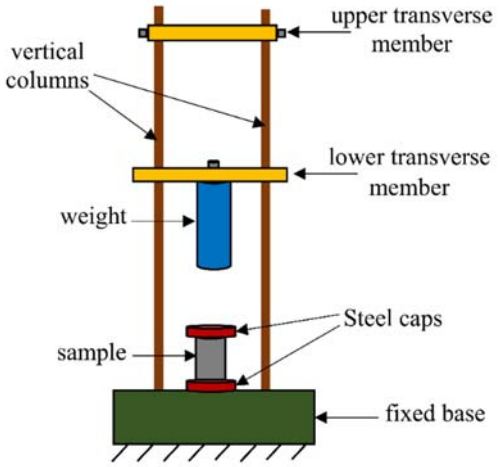

Figure 4 Schematic diagram of drop weight apparatus

Where I_1 and I_2 are acoustic impedances of steel and rock, ρ and c_L are mass density and wave velocity in each material. The cumulated energy (CE) in each step of impact loading without considering losses is $E = nmgh$, where *n* is the total number of applied successive impacts on the specimen, *m* is the mass of the impactor that falls from height *h* and $g = 10\ m/s^2$ is the gravity acceleration. On the other hand, if a striker with speed *V* hits at the cross section of a long elastic rod (or a cylindrical body), a dynamic compressive stress wave with the amplitude $\sigma_d = EV/v_p$ is produced in it which travels with speed $v_p = \sqrt{E/\rho}$ [19]. *E* is the elastic modulus of the rod (for bulk waves $v_p = \sqrt{(\lambda + 2\mu)/\rho}$, λ and μ being Lame' constants). By approximating the samples as long cylindrical bodies and neglecting the radial effects, using the data of samples, the impact velocities, strain rates, and stresses, corresponding to each falling height are calculated.

3.2 Fracture criteria

The fracture of some artificial models of porous rock under high strain rate loading indicates that initial porosity and the strain rate of loading affect the fracture of sample matrix [11]. Since the natural porous rock structure differs from the model structure and no other suitable fracture criterion for porous rock is found in the literature, the linear elastic fracture mechanics concept is applied to evaluate spall fracture conditions in test samples. In order to find out whether the stress waves in the present experiment can create fracture by spallation, samples have to be dealt with as elastic continuum materials [23]. The shear modulus, *G*, and the bulk modulus, *K*, are calculated using the relations between the Young's modulus E, and Poisson's ratio ν. These values are considered the same for all samples. The two criteria for spallation are the dynamic fracture strength criterion and the spall strength criterion [28]. According to the first criterion fracture will occur if the dynamic stress equals or exceeds the dynamic fracture strength σ_{xx} (Hugoniot Elastic Limit or HEL) which is calculated from Eq. (9):

$$\sigma_{xx} = \sigma_y (K/2G + 2/3) = \sigma_y (1-\nu)/(1-2\nu) \tag{9}$$

$\sigma_y = \sigma_t$ is the tensile strength.

The second criterion (Grady's energy criteria for fracture and fragmentation) states that spall fracture occurs if the sum of the strain energy and kinetic energy is at least as large as the fracture energy. In this treatment, Grady derived spall strength for brittle materials in terms of wave velocity c, fracture toughness K_c, and strain rate, $\dot{\varepsilon}$ as $P_s = (3\rho c K_c^2 \dot{\varepsilon})^{1/3}$. According to this criterion spall fracture occurs if dynamic stress equals or exceeds the spall strength. Values of K_c for some kinds of rock are listed in [30], but we estimate its value by using the measured tensile strength, σ_t as $K_c = \sigma_t \sqrt{\pi a}$. The parameter a, is the longest crack for the part that will not be discovered by the crack detection methods used in manufacture and in service [28]. We estimate a, as the minimum size of cracks and pores characterized by the resolution of SEM (Scanning Electronic Microscope) image, which is $2\mu m$ in our experiment.

4 Experiment measurements

Mechanical properties are determined in uniaxial compression test. Axial and lateral stress-strain diagrams are indicated in Figure (5). Compressive strength σ_{uc}, Young's modulus of elasticity (E_{50}), and Poisson's ratio ν, are 62.41MPa, 14.65GPa, and 0.37 respectively and the strain at compressive strength is 0.42%. The tensile strength is determined by Brazilian method as $\sigma_t = 5.17$ MPa. Dynamic response of hydraulic properties of porous rocks under stress waves produced by a falling weight, are analyzed by measuring the absolute gas permeability and effective porosity of plugs after each step of loading. Unsteady state Nitrogen permeameter based on Jones' Law [31] and Helium porosimeter based on Boyle's Law [32] are used for this purpose. Isolated pores and fractures play no role in these measurements.

The velocity of longitudinal and shear waves v_p, and v_s, are measured in a separate test by an ultrasound apparatus. A typical ultrasound echo is shown in Figure (6). Dynamic Poisson's ratio ν_d and elastic moduli G_d and E_d of the samples are calculated from the following relations [33]:

$$\nu_d = [(v_p/v_s)^2 - 2]/[2(v_p/v_s)^2 - 2] \tag{10}$$

$$G_d = \rho v_s^2, \quad E_d = 2(1+\nu_d)G_d \tag{11}$$

CT images are prepared in a scanner with parameters 120 kV X-ray tube voltage and 100 mA current. Image scanning for the whole plug is performed with total 12 seconds and the pixel size of images is 0.2 mm. Experiments are performed on reservoir rock samples obtained from a single core. Measured initial properties of samples are listed in Table (1). Figure (7) shows an intact sample of Asmari carbonate rock before testing and Scanning Electron Microscope (SEM) image in which pores and grains inside the sample are visible.

5 Experiment procedure

The experiment is carried out on three samples of reservoir rock core plugs from Ahvaz Asmari formation at southwest of Iran, under dry conditions and at room temperature (22°C ± 2°C). Loading is imposed on the samples in ten steps. The physical changes in sample properties are characterized by absolute gas permeability, effective porosity, wave velocities (v_p and v_s), and post-test X-ray computed tomography analysis. Mechanical properties are calculated from Eq.s (9) - (11). Variations of these properties are implemented after each step of loading and indicated as data points against cumulative energy (CE).

At the first step of loading, impactor falls on each one of the samples from heights 10, 20 and 30 centimeters imposing only one blow. The energy transferred into samples corresponding to the mentioned heights are 2, 4 and 6 N.m. Nevertheless the variation of absolute permeability, effective porosity and wave velocities were negligible and hence from second step onward, three successive blows are applied to the samples from mentioned heights.

The transferred energy is tripled and significant changes are observed in the absolute permeability of sample S72. To find out the physical structure changes in core plugs due to stress wave propagation, CT images of samples are prepared after each step. A similar test procedure is performed from second step up to seventh. Due to the insignificant changes of S70 absolute permeability, it was decided to increase the falling height for S70 and S71 samples to 30 cm for three remaining steps (input strain rate for these specimens increased). After the eighth step, the permeability of S70 increased considerably.

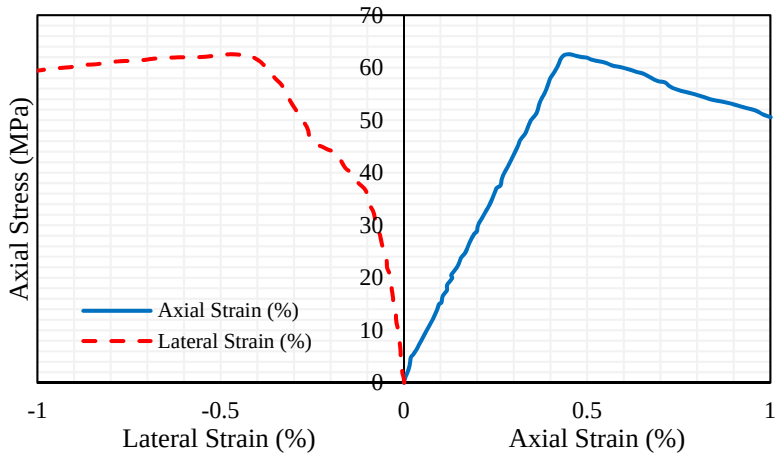

Figure 5 Uniaxial compression test diagram

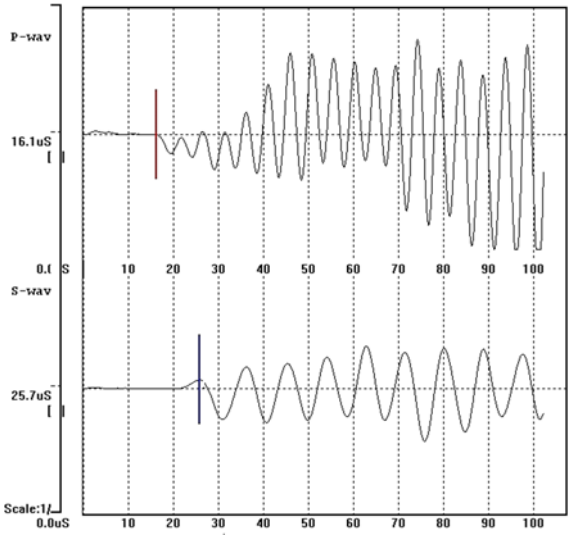

Figure 6 A typical ultrasound echo for measuring v_p and v_s in S70 sample

Table 1 Initial properties of samples measured under dry conditions

Sample code	Length (mm)	Diameter (mm)	Density (gr/cm^3)	Effective Porosity (%)	Absolute gas permeability (md)	v_p (m/s)	v_s (m/s)
S70	50.5	37	2.42	10.426	0.037	3130	1961
S71	50.4	37	2.45	9.572	0.039	3560	2000
S72	50	37	2.38	12.168	0.604	3106	1887

6 Results and Discussion

For W=20 N and t=3 mm an average transmission coefficient is calculated as T=0.274. The shear modulus, G, and the bulk modulus, K, are calculated as 5.35 GPa and 18.77 GPa respectively. The dynamic fracture strength $\sigma_{xx} = 12.52\,\text{MPa}$ and the fracture toughness $K_c = 12.96\times10^{-3}$ MP.m$^{1/2}$ have the same values for three samples (values of K_c are reported in [29] as $K_c = 0.657 - 0.992$ MP.m$^{1/2}$ for limestone and $0.180 - 0.198$ MP.m$^{1/2}$ for sandstone). The impact loading results using initial values at the first step of loading and the computed strengths are listed in Table (2). These results are determined after each step of loading and plotted as diagrams.

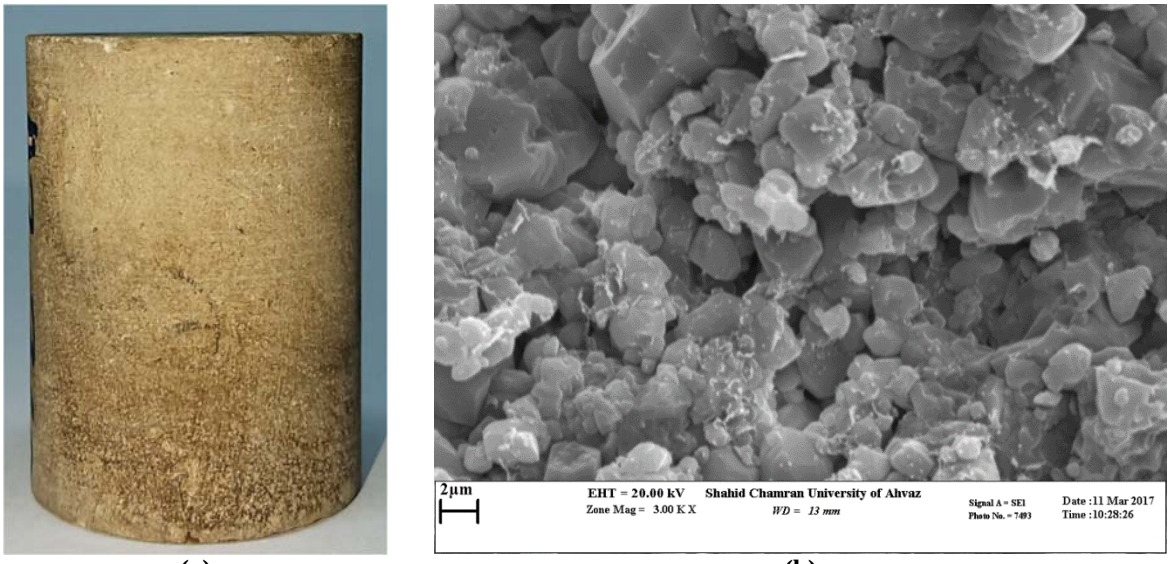

(a) **(b)**

Figure 7 Image of Asmari carbonate: **(a)** intact sample, **(b)** SEM

Table 2 Calculated values for three samples before experiment (step 0 of impact loading)

Sample code	*Falling height, h (cm)	Impact velocity, V (m/s)	Strain rate, $\dot{\varepsilon}_{rock}$ (s^{-1})	Dynamic stress amplitude, σ_d (MPa)	Equivalent static stress, σ_c (MPa)	Dynamic fracture strength, σ_{xx} (MPa)	Spall strength, P_s (MPa)
S70	10	1.4	129	6.56	35.55	12.52	0.8
S71	20	2	182.5	8.18	50.27	12.52	0.92
S72	30	2.45	223	11.5	61.56	12.52	0.94

*From 8th step onward h is increased to 30 cm for S70 & S71.

6.1 Strength criteria evaluation

In Figure (8) the dynamic stress amplitude, dynamic fracture strength, and spall strength of the samples are plotted against cumulative energy. It is clear that the dynamic stress exceeds both strengths and hence the two spall fracture criteria are fulfilled.

6.2 Absolute gas permeability variations

Variation of measured permeability of samples after each step of loading, versus CE are indicated in Figure (9). The absolute permeability of S70 had not sensible changes due to the low strain rate applied to it until the end of seventh step. By changing the test procedure and applying higher strain rate on S70 after eighth step, its absolute permeability increased 10 times of the seventh step. S71 absolute permeability had two considerable growth after fourth and eighth steps. After fourth step, absolute permeability was doubled against previous step and at the second time, by increasing the applied strain rate, it grew by 50%. Absolute permeability of S72 increased significantly after second step corresponding to 24 Nm CE and its incremental trend continued up to the end of impact loading steps. The ratio of mean absolute permeability of last steps of impact loading to their initial values are 10.1, 3.2 and 21.5 for S70, S71 and S72, respectively. Form these diagrams, it seems that significant increase in permeability will not be achieved until the cumulative energy density (cumulative energy per unit volume) reaches a certain thresh hold. This thresh hold for the samples S70, S71, and S72 are 0.68, 0.72, and 0.44 Nm/cm^3 respectively and depends on initial permeability of the sample and strain rate of incident stress wave.

6.3 Effective porosity variations

Figure (10) shows the effective porosity variation of each sample against CE. After the first step of loading the effective porosity drops significantly. The maximum reduction in effective porosity of S70, S71 and S72 relative to their initial values are 12.7%, 14.3%, and 12.8% respectively which may be due to breakage of the wall between active pores and hence the compaction of the rock. On the other hand, breaking the walls of isolated pores at the next steps of loading, will increase the pore volume by joining to other pores and micro fractures, leading to increase of effective porosity. This event is repeated more or less during the next steps of loading although the general trend indicates increase in effective porosity. Similar achievements are reported in [14, 34].

6.4 Wave velocity changes

Figure (11) shows the variation of longitudinal and shear wave velocities, v_p and v_s, in samples versus CE. Upward trend of these velocities indicate that the samples are compacted at first; which means the effective porosity of samples is reduced while downward trend indicate the presence of new fractures in the path of acoustic waves. The general trend indicates reduction in wave velocity against increasing cumulative energy.

6.5 Dynamic Young's and shear moduli changes

Figure (12) indicates the variation of dynamic Young's and shear moduli of each sample versus the wave velocities. The solid line shows the relation between one dimensional wave velocities and the corresponding modulus while the dotted line indicates the general trend of changes in Young's modulus and the measured longitudinal (bulk) wave velocity.

The measured values of velocities correspond to bulk waves and hence the computed values for dynamic Young's modulus are deviated from their theoretical (one dimensional) values to some extent. As was pointed out, the increase of cumulative energy leads to decrease in wave velocities (due to emerging new fractures) which indicate the reduction of samples moduli (reduction of strength to deformation). These diagram show that the shear wave velocity changes predict more accurately the changes in shear modulus.

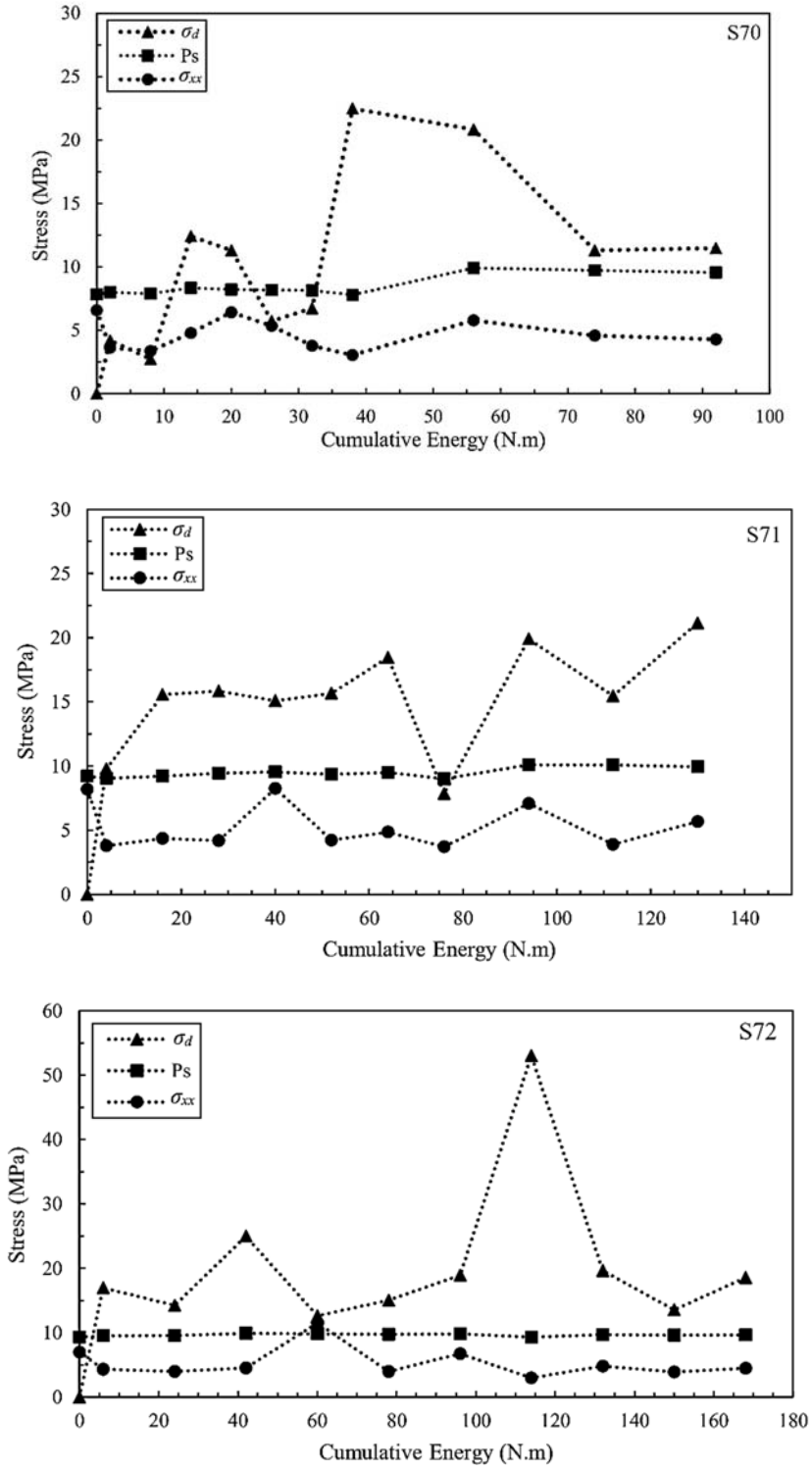

Figure 8 comparison of dynamic stress with sample strengths

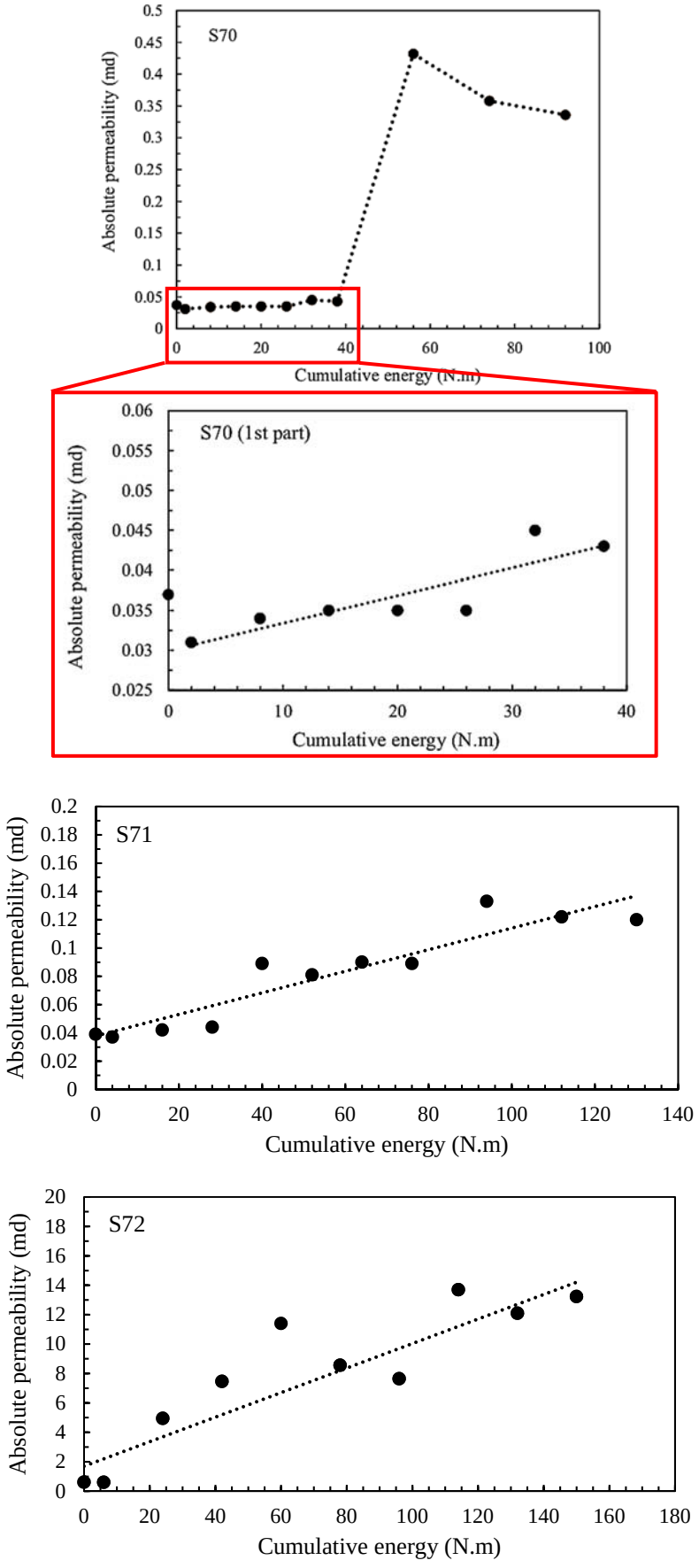

Figure 9 Variation of permeability due to cumulative energy

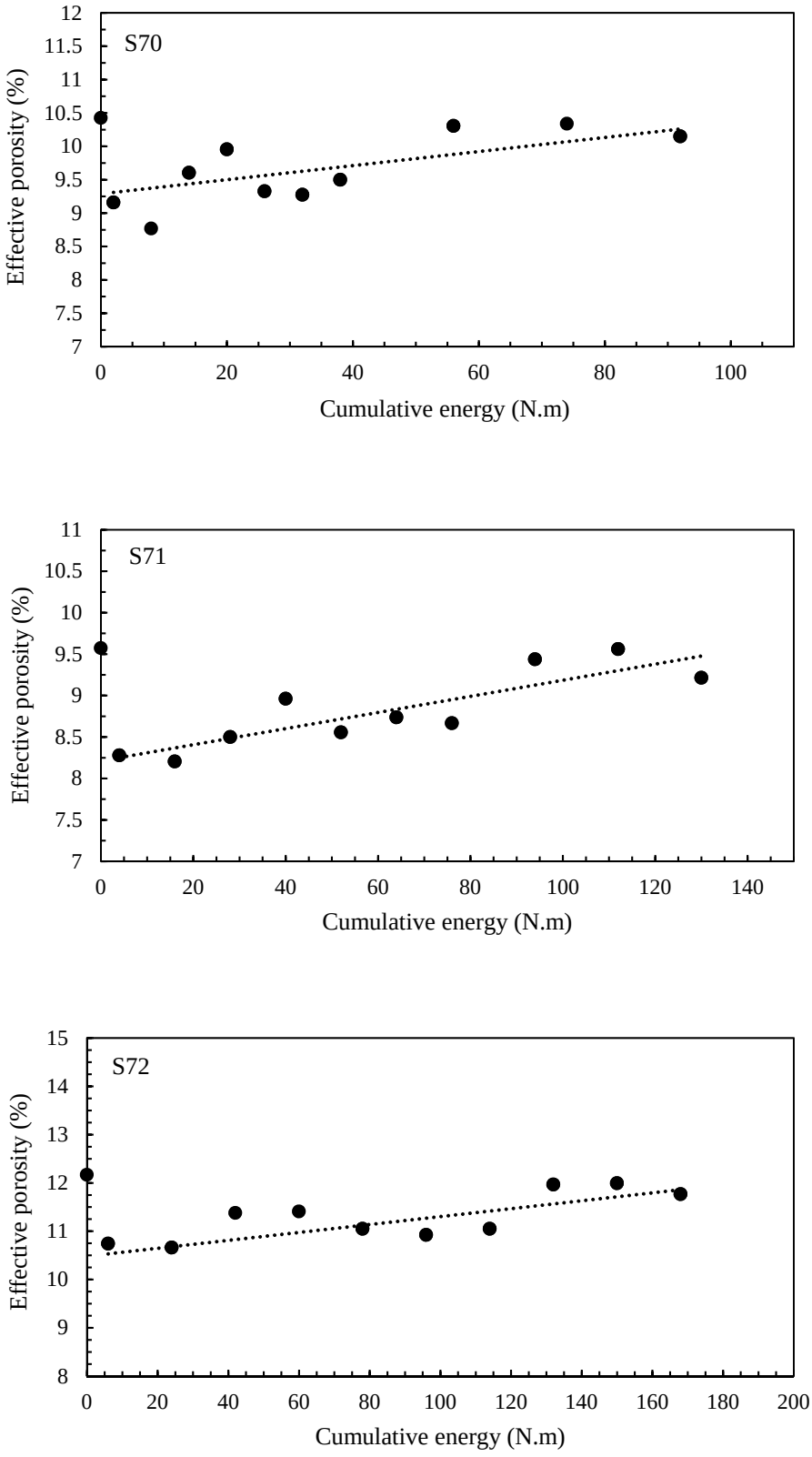

Figure 10 Variation of effective porosity due to cumulative energy

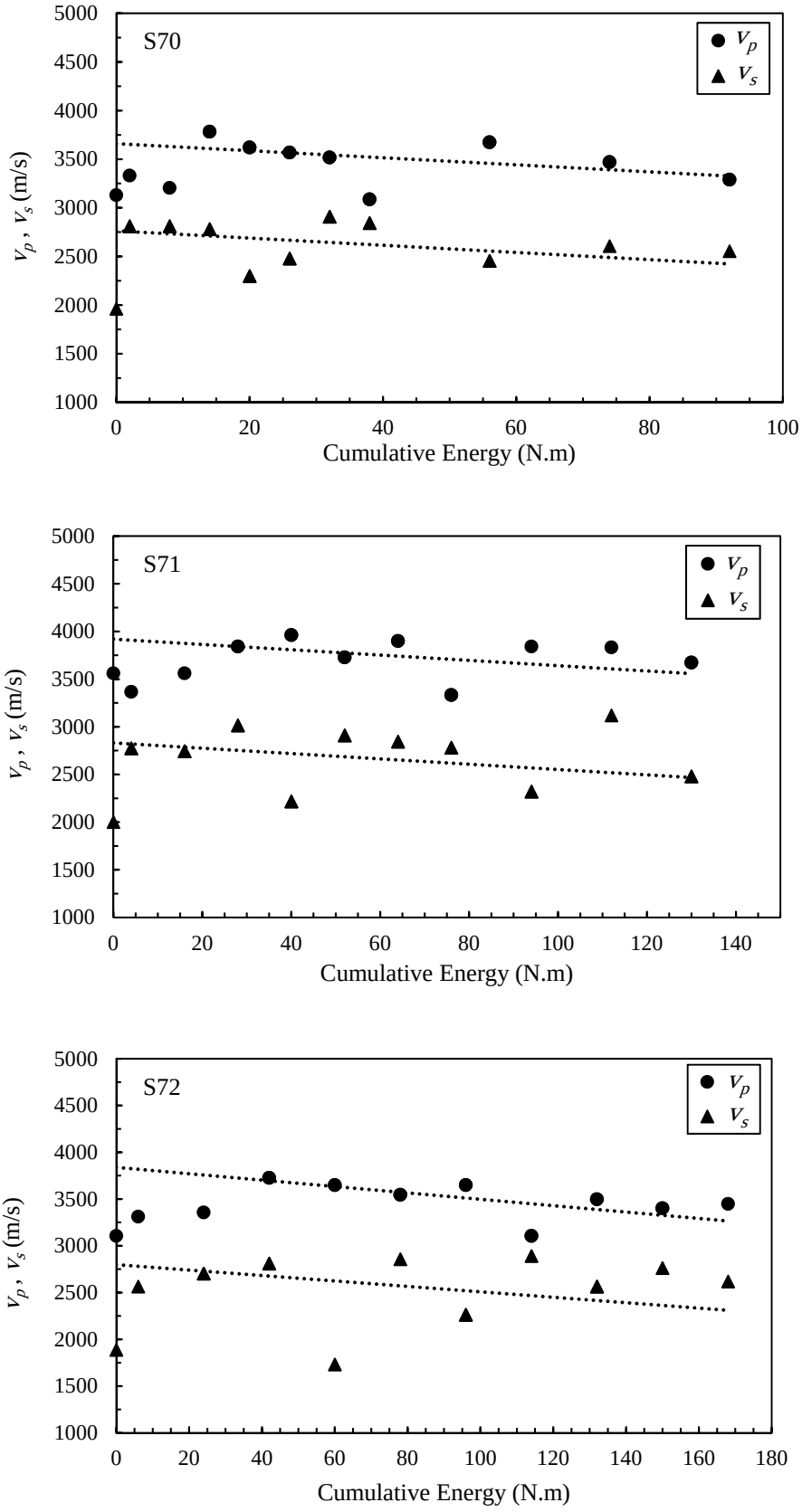

Figure 11 Wave velocity changes due to cumulative energy

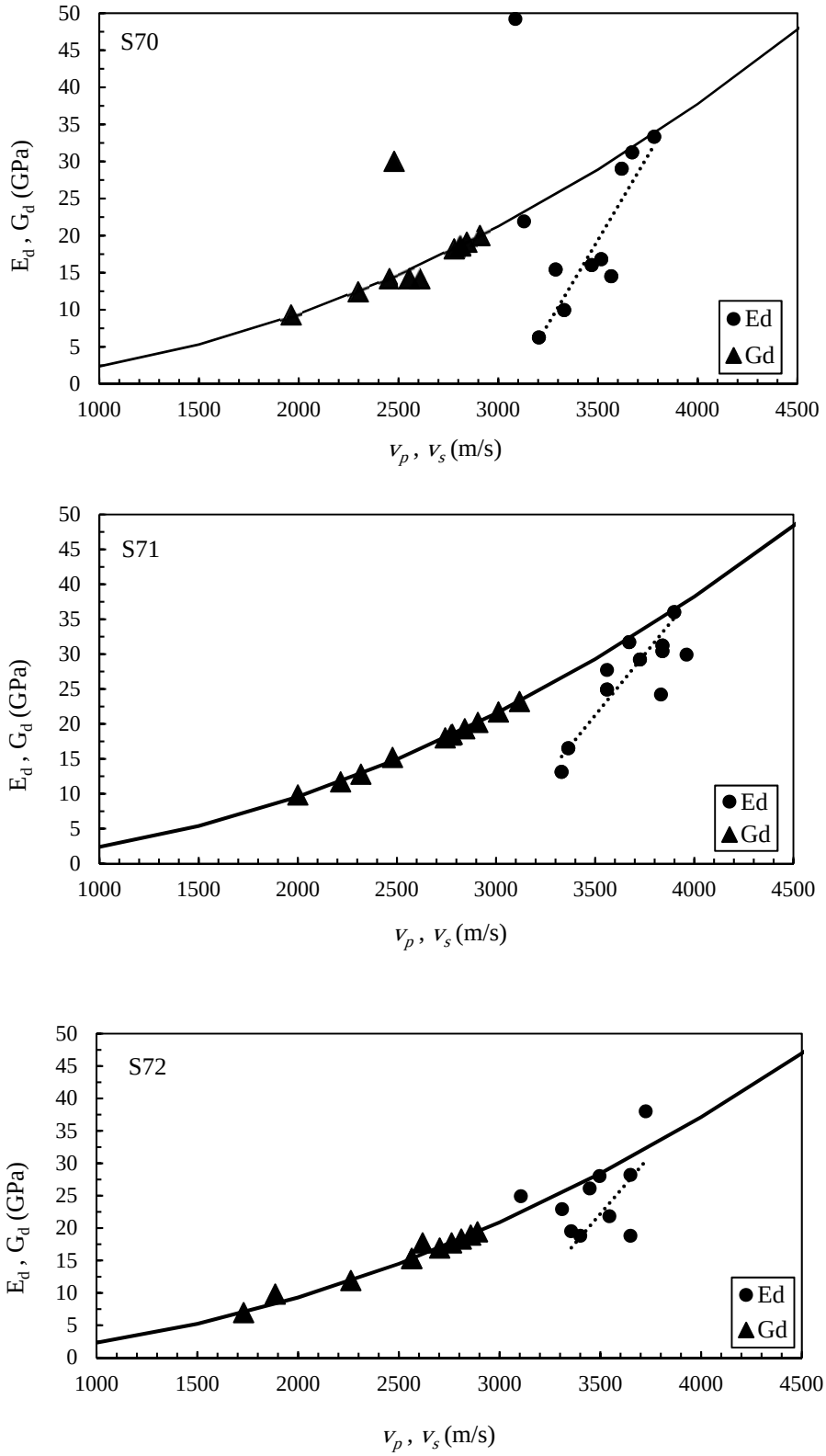

Figure 12 Variation of dynamic Young's and shear moduli with wave velocity

6.6 CT images

Selected pictures from generated fracture patterns or the growth of existing cracks due to impact loading visualized by CT images are shown in Figure (13). Samples S70 and S71 do not have visible cracks along the axis of core plugs although their absolute permeability changes due to generating invisible micro fractures. Visible cracks are observed in S70 after changing the applied strain rate (from eighth step onward). Sample S72 that received more CE with respect to other samples has more obvious fractures at the end of the test. Furthermore, visible crack initiation in this sample has been occurred earlier compared to other samples. Because of lengthwise cracks generated in S72, remarkable increase in its permeability is observed.

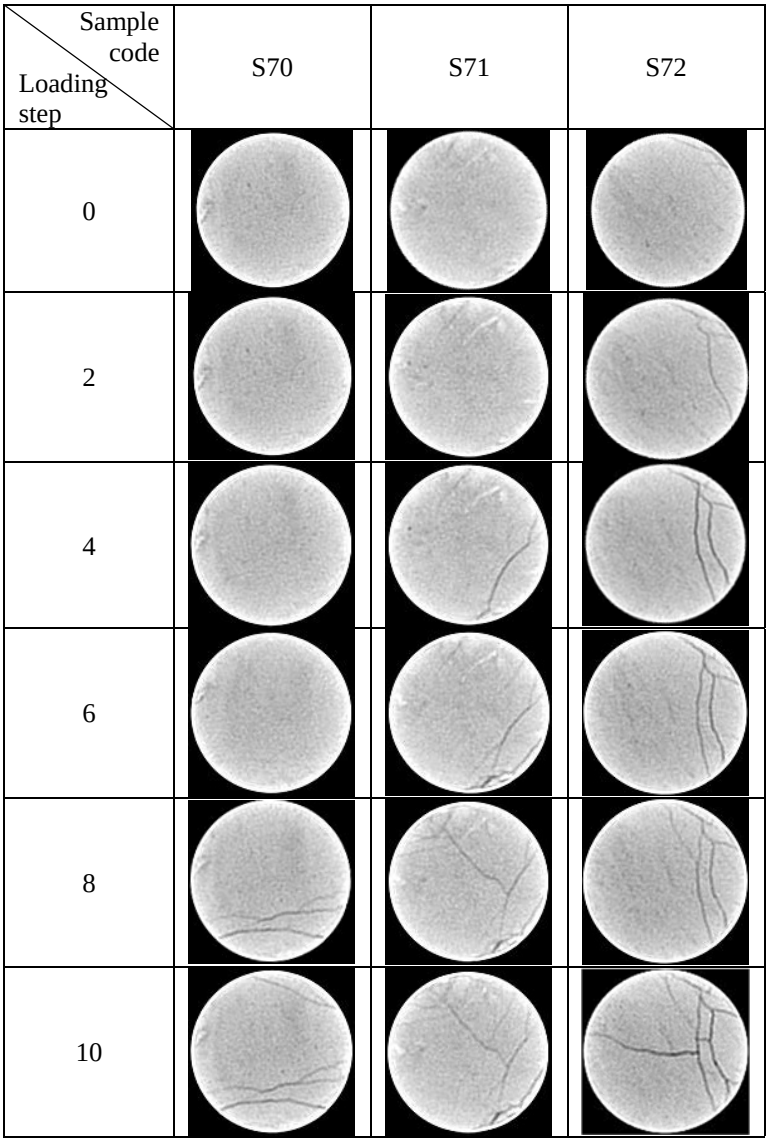

Figure 13 Fracture patterns generated inside the porous samples by successive impact loading visualized by X-ray CT images

7 Conclusion

The effects of repetitive impact loading on the various properties of reservoir rock samples are studied. Three reservoir carbonate rock plugs from Asmari formation are loaded in a drop weight apparatus repetitively. Impact loading induces compressive stress wave in the samples which interact with pore and fracture surfaces. Considering the samples dry and free from any fluid and no confining pressure, the interaction of these waves with stress free surfaces of pores and fractures are investigated. The dynamic stress of the wave is compared with the dynamic fracture strength and spall strength of the rock samples to evaluate the fracture criteria. The results show that:

- The dynamic stress is high enough to produce additional fractures in the rock samples and hence is capable to affect such properties as absolute gas permeability and effective porosity of reservoir rock.
- The higher the compressive stress wave amplitude and its strain rate, the higher density and longer micro fractures are developed inside the porous rock samples leading to changes in their structural integrity and hydraulic properties.
- The ratio of mean absolute permeability of the samples at the last step of impact loading to their initial values increases significantly.
- The effective porosity of the samples increases after a sudden decrease during the initial steps of loading.
- Longitudinal and shear wave velocities increase during the initial steps of loading but decrease afterwards, indicating a general decreasing trend.
- Increasing the wave velocity at first stages of loading is an indication of closing apertures or collapsing and compaction of pores while decreasing of wave velocity is an indication of emerging new fractures in the path of wave motion.
- The CT images indicate that the density and length of micro fractures will increase at higher steps of the loading that are characterized by higher cumulated energy.
- Due to impact loading on the porous rock, a new system of cracks by spallation and stress concentration is formed within the sample that create new passages.
- The idea of imposing successive compressive stress waves with high enough amplitude at suitable locations of a reservoir, may improve oil recovery.

Experiments on samples saturated with fluid under confined pressure are needed in order to generalize the results of present research.

Acknowledgement

This research is supported partially by Research Council of Shahid Chamran University of Ahvaz [grant number 97/3/02/26247] and Iran National Science Foundation (INSF) [grant number 96001474, 2017]. The authors also gratefully acknowledge The Research & Technology of National Iranian South Oil Company (NISOC) for delivering reservoir rock samples and Central laboratories of Shahid Chamran University of Ahvaz for preparing SEM images.

References

[1] Eakin J.L., and Miller J.S., “Explosives Research to Improve Flow Through Low-permeability Rock”, Journal of Petroleum Technology, Vol. 19, pp. 1431-1436, (1967).

[2] Khelifa, C., Zeddouri, A., and Djabes, F., "Influence of Natural Fractures on Oil Production of Unconventional Reservoirs", Energy Procedia, Vol. 50, pp. 360-367, (2014).

[3] Hunt III, W., and Shu, W., "Controlled Pulse Fracturing for Well Stimulation", Low Permeability Reservoirs Symposium, Colorado, (1989).

[4] Abramova, A. V., Abramov, V. O., Kuleshov, S. P., and Timashev, E. O., "*Analysis of the Modern Methods for Enhanced Oil Recovery*", in Sharma, U. C., Kumar, S., Prasad, R., Govil, J. N., (Editors), Energy Science and Technology, Vol. 3, pp. 118-148, Studium Press, USA, (2014).

[5] Gandossi, L., and Von Estorff, U., "An Overview of Hydraulic Fracturing and other Formation Stimulation Technologies for Shale Gas Production-update 2015", EUR 26347, Publications Office of the European Union, Luxembourg, pp. 1-62, (2015).

[6] Pijaudier-Cabot, G., Borderie, C. L., Reess, T., Chen, W., Maurel, O., Rey-Berbeder, F., and de Ferron, A., "*Electrohydraulic Fracturing of Rocks"*, Wiley, Great Britain, (2016).

[7] Causin, E., "*Enhanced Oil Recovery*", in Encyclopaedia of Hydrocarbons, Vol. III/ New Developments: Energy, Transport, Sustainability, ENI, Rome, (2007).

[8] Abramova, A., Abramova, V., Bayazitov, V., Gerasin, A., and Pashin, D., "Ultrasonic Technology for Enhanced Oil Recovery", Engineering, Vol. 6, pp. 177-184, (2014).

[9] Dysart, G., Spencer, A., and Anderson, A., "Blast-fracturing", Drilling and Production Practice Conference, January 1st, Washington, D.C., pp. 68-76, (1969).

[10] Spencer, A., Dysart, G., and Anderson, A., "New Blasting Methods Improve Oil Recovery", SPE Practical Aspects of Improved Recovery Techniques Symposium, pp. 1-12, Texas, March 8-9, (1970).

[11] Rinehart, J.S., "Fracturing by Spalling", Wear, Vol. 7, pp. 315-329, (1964).

[12] Dong, Y. X., Xia, C. J., Xiao, L. X., and Feng, S. S., "Dynamic Mechanical Properties of Porous Rock under Impact Loading", Advanced Materials Research, Vol. 228-229, pp. 5-9, (2011).

[13] Zou, F., Fang, Z. F., and Xia, M. Y., "Study on Dynamic Mechanical Properties of Limestone under Uniaxial Impact Compressive Loads", Mathematical Problems in Engineering, Vol. 2016, pp. 1-11, (2016).

[14] Ju, Y., Yang, Y.M., Mao, Y.Z., Liu, H.B., and Wang, H.J., "Laboratory Investigation on Mechanisms of Stress Wave Propagations in Porous Media", Science in China Series E: Technological Sciences, Vol. 52, pp. 1374-1389, (2009).

[15] Zhang, Q. B., and Zhao, J., "Quasi-static and Dynamic Fracture Behaviour of Rock Materials: Phenomena and Mechanisms", International Journal of Fracture, Vol.189, pp. 1-32, (2014).

[16] Zhang, Q. B., and Zhao, J., "A Review of Dynamic Experimental Techniques and Mechanical Behaviour of Rock Materials", Rock Mechanics and Rock Engineering, Vol. 47, pp. 1411-1478, (2014).

[17] Li, S.H., Zhu, W.C., Niu, L.L., Yu, M., and Chen, C.F., "Dynamic Characteristics of Green Sandstone Subjected to Repetitive Impact Loading: Phenomena and Mechanisms", Rock Mechanics and Rock Engineering, Vol. 51, pp. 1921-1936, (2018).

[18] Tong, L.H., Yu, Y., Lai, S.K., and Lim, C.W., "Dynamic Weakening of Sandstone Subjected to Repetitive Impact Loading", Rock Mechanics and Rock Engineering, Vol. 52, pp. 2197-2206, (2019).

[19] Timoshenko, S.P., and Goodier, J.N., "*Theory of Elasticity*", 3rd Edition, McGraw-Hill, New York, (1970).

[20] Wang, L., "*Foundations of Stress Waves*", 1st Edition, Elsevier Science, Great Britain, (2011).

[21] Graff, K.F., "*Wave Motion in Elastic Solids*", Dover Publication, New York, (2012).

[22] Biot, M.A., "Theory of Propagation of Elastic Waves in a Fluid-saturated Porous Solid", Journal of the Acoustical Society of America, Vol. 28, pp. 168-191, (1956).

[23] Rossmanith, H.P., and Uenishi, K., "The Mechanics of Spall Fracture in Rock and Concrete", Fragblast, Vol. 10, pp. 111-162, (2006).

[24] Antoun, T., Curran, D.R., Seaman, L., Kanel, G.I., Razorenov, S.V., and Utkin, A.V., "*Spall Fracture*", Springer, NewYork, (2003).

[25] Jacobsson, L., Appelquist, K., and Lindkvist, J. E. "Spalling Experiments on Large Hard Rock Specimens", Rock Mechanics and Rock Engineering, Vol. 48, pp. 1485-1503, (2015).

[26] Kim, Y.M., Lee, B.H. and Ih, J.G., "Scattering of Longitudinal Waves by a Cylindrical Cavity in an Attenuating Solid", The Journal of the Acoustical Society of America, Vol. 93, pp. 93-101, (1993).

[27] Khedri, M., "Investigation of Ultrasonic Scattering around Cylindrical Cavity in Elastic Medium", M.Sc. Dissertation, Department of Mechanical Engineering, Facultu of Engineering, Shahid Chamran University of Ahvaz, Iran, (2015).

[28] Shigley, J.E., and Mischke, C.R., "*Mechanical Engineering Design*", McGraw-Hill, New York, (1989).

[29] Rose, J.L., "*Ultrasonic Waves in Solid Media*", Cambridge University Press, Cambridge, UK, (2004).

[30] Rossmanith, H.P., "*Rock Fracture Mechanics*", Springer, Vienna, (2014).

[31] Jones, S.C., "A Rapid Accurate Unsteady-state Klinkenberg Permeameter", Society of Petroleum Engineers Journal, Vol. 12, pp. 383-397, (1972).

[32] Bear, J., "*Dynamics of Fluids In Porous Media*", Dover, New York, (1988).

[33] Mavko, G., Mukerji, T., and Dvorkin, J., "*The Rock Physics Handbook: Tools for Seismic Analysis of Porous Media*", 2nd Edition, Cambridge University Press, New York, (2009).

[34] Torsæter, O., and Abtahi, M., "*Experimental Reservoir Engineering Laboratory Work Book*", Norwegian University of Science and Technology: Department of Petroleum Engineering and Applied Geophysics, Norway, (2003).

Nomenclature

a	Radius of spherical cavity, Incident wave amplitude, Crack length
A_n	Constant coefficient
B_n	Constant coefficient
CE	Cumulative energy
c_L, v_p	Longitudinal wave velocity
v_s	Transverse wave velocity
E	Elastic (Young's) modulus
E_d	Dynamic Elastic (Young's) modulus
F	Static force
g	Gravity acceleration
G	Shear modulus
G_d	Dynamic Shear modulus
h	Falling height
h_n	First kind spherical Bessel function
i	Complex number
I	Acoustic impedance
j_n	First kind spherical Hankel function
k	Stiffness
K	Bulk modulus
K_c	Fracture toughness
m	Striker mass, an integer
n	Number of successive impacts, iteration number
P_n	Legendre function
P_s	Spall strength
r	Distance from spherical cavity center
t	Time, Steel cap thickness
T	Transmission coefficient
V	Impactor velocity

W	Striker weight
x	Distance from stress free surface

Greek symbols

α, k_l	Longitudinal wave number
β, k_t	Transverse wave number
$\dot{\varepsilon}$	Strain rate
φ_0	Amplitude of incident potential function
λ	Lame' coefficient, Wave length
μ	Lame' coefficient
ν	Poisson ratio
ν_d	Dynamic Poisson ratio
ρ	Density
σ_c, σ_{uc}	Compressive stress
σ_d	Dynamic stress amplitude
$\sigma_{rr}, \sigma_{r\theta}$	Radial and shear component of stress field
σ_t, σ_y	Tensile strength
σ_{xx}	Dynamic fracture strength
ω	Frequency